Astronomy & Astrophysics

On the nature of the Cygnus X-2 like Z-track sources

M. Bałucińska-Church[1,2], A. Gibiec[2], N. K. Jackson[1], and M. J. Church[1,2]

[1] School of Physics and Astronomy, University of Birmingham, Birmingham, B15 2TT, UK
  e-mail: mbc@star.sr.bham.ac.uk
[2] Astronomical Observatory, Jagiellonian University, ul. Orla 171, 30-244 Cracow, Poland

ABSTRACT

Based on the results of applying the extended ADC emission model for low mass X-ray binaries to three Z-track sources: GX 340+0, GX 5-1 and Cyg X-2, we propose an explanation of the Cygnus X-2 like Z-track sources. The Normal Branch is dominated by the increasing radiation pressure of the neutron star caused by a mass accretion rate that increases between the soft apex and the hard apex. The radiation pressure continues to increase on the Horizontal Branch becoming several times super-Eddington. We suggest that this disrupts the inner accretion disk and that part of the accretion flow is diverted vertically forming jets which are detected by their radio emission on this part of the Z-track. We thus propose that high radiation pressure is the necessary condition for the launching of jets. On the Flaring Branch there is a large increase in the neutron star blackbody luminosity at constant mass accretion rate indicating an additional energy source on the neutron star. We find that there is good agreement between the mass accretion rate per unit emitting area of the neutron star $\dot{m}$ at the onset of flaring and the theoretical critical value at which burning becomes unstable. We thus propose that flaring in the Cygnus X-2 like sources consists of unstable nuclear burning. Correlation of measurements of kilohertz QPO frequencies in all three sources with spectral fitting results leads to the proposal that the upper kHz QPO is an oscillation always taking place at the inner accretion disk edge, the radius of which increases due to disruption of the disk by the high radiation pressure of the neutron star.

Key words. accretion, accretion disks – stars: neutron – X-rays: binaries – X-rays: individuals: Cyg X-2 –
X-rays: individuals: GX 340+0 – X-rays: individuals: GX 5-1

1. Introduction

The Z-track sources are the brightest group of Galactic low mass X-ray binaries (LMXB) containing a neutron star persistently emitting at the Eddington luminosity or several times this. The sources trace out a Z-shape in hardness-intensity or hardness-softness (Hasinger & van der Klis 1989) having three branches labelled the horizontal branch (HB), the normal branch (NB) and flaring branch (FB). Strong physical changes are clearly taking place at the inner disk and neutron star, but a generally accepted explanation of the Z-track phenomenon has not existed. Hasinger & van der Klis (1989) presented colour-colour diagrams for all six original Z-track sources using *Exosat* data which showed rather different shaped Z-tracks between two groups: Cyg X-2, GX 340+0 and GX 5-1 (the Cygnus X-2 like sources) and Sco X-1, GX 17+2 and GX 349+2 (the Sco X-1 like sources). It was proposed that these constituted two sub-groups of Z-track sources, for example by Kuulkers et al. (1994), and this became generally accepted (Kuulkers & van der Klis 1995; Smale et al. 2000, 2003). Many observations have confirmed the rather different shaped Z-tracks, the Cygnus X-2 like sources having a long HB, while the Sco X-1 like sources have a short HB but a long FB.

LMXB have been classified according to the various phenomena observed, into the Atoll, Z-track, dipping and ADC sources, and this has been shown to relate to inclination angle so that X-ray dipping is seen at inclinations greater than ~65°. The Z-track sources display characteristic patterns in hardness-intensity but, in general, no orbital related behaviour indicating smaller inclination and the Atoll sources exhibit rather different patterns of hardness-intensity. However, a more basic classification would be based on luminosity in which the Z-track sources have luminosities greater than ~10^{38} erg s^{-1} and the Atoll sources have luminosities between ~10^{36} and ~10^{38} erg s^{-1}, although not all lower luminosity LMXB have been identified as Atoll sources via their hardness-intensity patterns. These patterns are also not understood, nor is the relation between the Z-track and Atoll classes, so that understanding Z-track and Atoll sources remains a fundamental problem.

Thus we need to understand the detailed nature of the inner disk and accretion in the super-Eddington LMXB, the Z-track sources, but these are also important since they are detected as radio emitters, although essentially in one part of the Z-track only: the horizontal branch. Not only is radio detected, but striking results from the VLA show the release of massive radio condensations from the source Sco X-1 (Fomalont et al. 2001) moving outwards in two opposite direction at velocity $v/c \sim 0.45$. Because radio is detected essentially in one branch only, the sources offer the possibility of determining conditions pertaining inside the sources via X-ray observations, i.e. the conditions at the inner disk, when jets are present, which distinguish the horizontal branch from the other branches, and so finding the conditions necessary for jet formation.

Possible ways of understanding the Z-track sources are by timing studies, spectral studies or theoretical studies. Extensive timing studies have been made to investigate the quasi periodic oscillations (QPO) found in the Z-track and other sources (e.g. van der Klis et al. 1987). This has revealed a wealth of complex behaviour, and in particular, study of the kilohertz QPO has

Article published by EDP Sciences

revealed a pattern of variation of the twin kHz peaks on the horizontal branch of Z-track sources, and various models have been proposed to explain the QPO (Stella & Vietri 1998; Abramowicz & Kluźniak 2001; Miller et al. 1998). However, it is difficult to determine what changes take place at the inner disk around the Z-track from data on the kHz QPO.

Previous spectral fitting tended to apply a particular LMXB emission model: the Eastern model of Mitsuda et al. (1989) in which the emission is assumed to consist of disk blackbody emission plus Comptonized emission from the neutron star or inner disk. Application of this model may have given acceptable fits to the spectra (Done et al. 2002; Agrawal & Sreekumar 2003; di Salvo et al. 2002), however, interpretation of the results, i.e. of the variation of the various spectral parameters around the Z-track was not easy. Our previous work over an extended period on the dipping class of LMXB provided evidence for a different emission model and we proposed the "extended ADC (accretion disk corona)" model (Church & Bałucińska-Church 2004, 1995) in which the emission components consist of blackbody emission from the neutron star plus Comptonized emission from an extended ADC. In this model, the ADC covers a substantial fraction of the inner disk and the thermal emission of the disk provides the seed photons for Comptonization (Church & Bałucińska-Church 2004). The model was developed from longterm studies of the dipping LMXB sources. In all LMXB, the observed shape of the spectrum and spectral fitting show that Comptonized emission dominates the spectrum, i.e. comprises more than 90% of the total luminosity, as shown for example in the *ASCA* survey of LMXB of Church & Bałucińska-Church (2001). In less luminous sources, the percentage may be higher, while in the brightest sources, the Z-track sources, the contribution is ∼90% at the soft apex. In the dipping sources, it is generally accepted that the reductions in X-ray intensity at the orbital period are due to absorption in the bulge in the outer accretion disk (White & Swank 1982; Walter et al. 1982). Spectral fitting of non-dip and dip spectra clearly shows that the dominant Comptonized spectral component is removed only slowly in dipping and so the 90% contributor to the total luminosity must be extended (e.g. Church et al. 1997). Measurement of the dip ingress times provides the sizes of the extended emission. These measurements indicated the radial extent to be very large: between 20 000 and 700 000 km depending on source luminosity (Church & Bałucińska-Church 2004). Moreover, this extended region cannot reach very high above the disk otherwise it would not be possible to fully cover the emitter by absorber and 100% deep dipping, often observed, would not be possible. Thus the conclusion cannot be avoided that 90% of the total luminosity originates in this extended region which, given the measured geometry: large in radial extent but small in height, can be identified with a hot, thin accretion disk corona above the disk, typically extending across 15% of the disk radius. Recently independent support for the model came from the *Chandra* grating results of Schulz et al. (2009) on Cyg X-2. Precise grating measurements revealed a wealth of emission lines of highly excited states such as the H-like ions of Ne, Mg, Si, S and Fe. The width of these lines indicated Doppler shifts due to orbital motion in the accretion disk corona at radial positions between 18 000 and 110 000 km in good agreement with the overall ADC size from dip ingress timing. Further support for line formation at large radial distances in an extended ADC came from recent results of *Chandra* observations of 4U 1624-490 (Xiang et al. 2009). The evidence for the extended corona is thus now overwhelming.

Theoretical modelling for the Z-track sources was carried out by Psaltis et al. (1995) assuming a magnetosphere of the neutron star and the changing properties and geometry of this as the mass accretion rate changed. However, the model assumed that the Comptonized emission observed in the spectra of all LMXB originated in a small central region close to the neutron star, not in an extended region.

It should also be stated here that although the nature of the Z-track has not been clear, there has been a standard assumption made that the mass accretion rate increases monotonically around the Z-track in the sense HB-NB-FB, based originally on results from multi wavelength observations of Cygnus X-2 (Hasinger et al. 1990). This assumption has been widely but not universally adopted and it will appear in Sects. 3 and 4 that our results do not support this assumption.

More recently, we have taken the approach of applying the extended ADC model to the Z-track sources GX 340+0 (Church et al. 2006) and GX 5-1 (Jackson et al. 2009), on the basis that the evidence favours the Extended ADC model, to test the hypothesis that this can fit the spectra, and provide a physically reasonable and consistent explanation of the Z-track. Good fits to the spectra at all positions on the Z-track were obtained, and the spectral fitting clearly suggested an explanation of the physical changes taking place on the Z-track. At the Soft Apex: the junction of the HB and FB, the X-ray intensity is minimum. Ascending the normal branch to the Hard Apex, the intensity increases substantially and the neutron star blackbody temperature kT increases from ∼1 to ∼2 keV. The luminosity of the ADC Comptonized emission (L_{ADC}) which is 90% of the total 1–30 keV luminosity at the soft apex increases by a factor of two or more strongly suggesting that $\dot{M}$ was increasing. The increase of kT is consistent with this and has a major consequence that the radiation pressure of the neutron star ($\sim T^4$) increases by an order of magnitude. The strength of the radiation pressure close to the neutron star which will determine its effects on the inner accretion disk is conveniently expressed in terms of the ratio of the flux emitted per unit area to its Eddington value f/f_{Edd} where $f_{Edd} = L_{Edd}/4\pi R^2$ and R is the radius of the neutron star. This ratio is a better measure of radiation pressure effects close to the neutron star than L/L_{Edd} which averages the flux over the surface, especially if only part of the surface is emitting. In GX 340+0, f/f_{Edd} was found to increase from 0.2 at the soft apex to 1.5 at the hard apex rising to almost 3 times super-Eddington on the HB. In GX 5-1 the ratio similarly increased to become greater than unity, so that in both sources, the radiation became super-Eddington at the hard apex and HB. It is these parts of the Z-track on which jets are observed and we proposed that the high radiation pressure disrupts the inner disk and drives matter into the vertical direction so launching the jets (Church et al. 2006; Jackson et al. 2009).

In both sources, on the flaring branch L_{ADC} was constant suggesting $\dot{M}$ was constant, while the neutron star blackbody luminosity increased strongly implying that a non-accretion powered energy source developed on the neutron star. The mass accretion rate per unit area of the neutron star $\dot{m} = \dot{M}/4\pi R^2_{BB}$, where R_{BB} is the blackbody radius derived from spectral fitting, was found at the start of the FB, i.e. the soft apex, to be in good agreement with the theoretical critical value $\dot{m}_{ST}$ (Bildsten 1998). This is the critical value of $\dot{m}$ below which nuclear burning on the surface of the neutron star becomes unstable, i.e. for $\dot{m} < 1.3 \times 10^5$ g cm^{-2} s^{-1} the burning changes from stable to unstable. Thus it was proposed that for a source descending the normal branch with falling $\dot{M}$, the onset of unstable burning causes the strong flaring seen in the X-ray lightcurve. The increase in blackbody luminosity is simply the nuclear burning power, as seen at essentially constant L_{ADC}, i.e. constant $\dot{M}$.
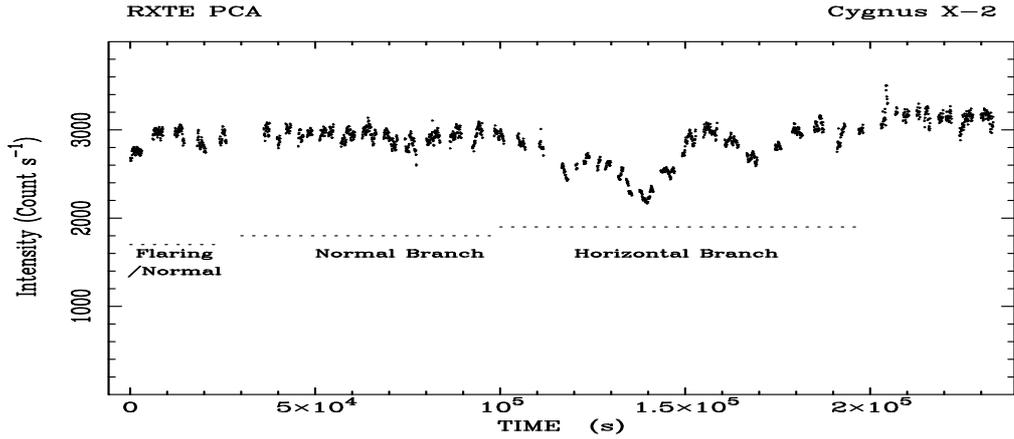
Fig. 1. Background-subtracted and deadtime-corrected PCA light curve of Cygnus X-2 with 64 s binning.

In the second source, GX 5-1, the evolution of the kilohertz QPO was also investigated by Jackson et al. (2009). Using the same selections of data used in spectral analysis, the variation of the kHz QPO along the HB and part of the NB was obtained by timing analysis, and viewed in the light of the spectral fitting results. It is well-known that the upper and lower kHz QPO frequencies ν_2 and ν_1 vary on the HB (e.g. Jonker et al. 2000; Wijnands et al. 1998a,b), and that if ν_2 is assumed to correspond to a Keplerian frequency in the disk, the radial position r is ~18 km, i.e. some way into the disk. A previously unknown correlation was found between the measured frequencies and the above ratio f/f_{Edd} (Jackson et al. 2009), specifically that the r was approximately constant until $f/f_{Edd} = 1$, above which r increased rapidly. This supports the proposal of disk disruption by high radiation pressure; moreover it suggests a mechanism for the upper frequency kHz QPO that this oscillation is always an oscillation at the inner disk edge, the radius of which was modified by different levels of radiation pressure. Thus disruption of the inner disk was the factor determining the frequency of the higher frequency kHz QPO and its variation.

In this work, we apply the extended ADC model for the first time to the Z-track source Cygnus X-2, also determining the evolution of the kHz QPO around the Z-track in Cyg X-2 and in GX 340+0 and we present a comparison of the three Cygnus X-2 like sources.

2. Observations and analysis

We analysed the *Rossi-XTE* observation of Cygnus X-2 of June 30–July 3, 1997 in which a full Z-track was covered in a relatively short time. The observation consisted of 11 sub-observations spanning 235 ks. Data from both the proportional counter array (PCA: 2–60 keV) and the high energy X-ray timing experiment (HEXTE: 15–250 keV) were used. PCA data in Standard2 mode with 16 s resolution were used for the extraction of light curves and spectra. Examination of the housekeeping data showed that three of the five Xe proportional counter units (PCUs) were consistently on, and so data were extracted from these (PCUs 0, 1 and 2). Standard screening criteria were applied to select data with an offset between the source and telescope pointing direction of less than 0.02° and elevation above the Earth's limb greater than 10°. Data were extracted from the top layer of the detectors using both left and right anodes. Analysis was carried out using the standard *RXTE* software FTOOLS 5.3.1. A lightcurve was generated in the band 1.9–20.3 keV and the facility PCABACKEST used to generate background files for each
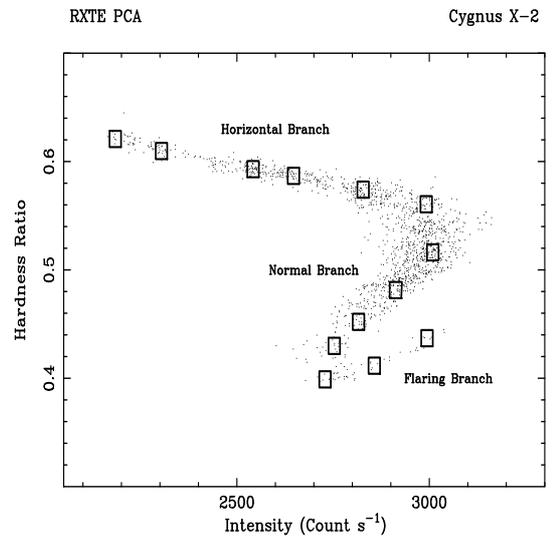

Fig. 2. Hardness ratio (7.3–18.1 keV)/(4.1–7.3 keV) variation with intensity.

raw data file based on the latest bright-source background model for Epoch 3 of the mission during which the observations were made. Deadtime correction was carried out, and the background-subtracted, deadtime-corrected lightcurve is shown in Fig. 1 with 64 s binning. Lightcurves were also extracted in three sub-bands: 1.9–4.1, 4.1–6.9 and 6.9–20.3 keV. By dividing the high band by the medium band lightcurve, a hardness-intensity plot was made as shown in Fig. 2. Individual subsections of the lightcurve were identified with their positions on the Z-track by making a hardness-intensity plot for each and locating its position on the overall Z-track. Thus the three Z-track branches are identified as shown in Fig. 1.

Lightcurves and spectra were also extracted from Cluster 1 and Cluster 2 of the HEXTE instrument, so that simultaneous spectral fitting of PCA and HEXTE spectra could be carried out. These were extracted with the FTOOL HXTLCURV which also provided background files and allowed deadtime correction.

Timing analysis was carried out as a function of position along the Z-track. The data used for this were single bit data of type SB_125us_14_249_1s, i.e. data having 125 μs resolution and a single energy bin spanning 5–60 keV. Power density spectra were extracted for each selection on the Z-track using the *Xronos* facility POWSPEC in a single energy bin, and Leahy

normalization was applied. To allow high quality fitting of the spectra, they were converted to a format allowing use of the *Xspec* spectral fitting software, by modifying the file headers and re-naming of columns. FLX2XSP was used to produce a file with the required *pha* extension and to generate a dummy instrument response as needed by *Xspec* consisting of a unitary matrix having no effect on the data. The spectra were grouped to a minimum count per bin to allow use of the χ^2 statistic, the grouping varying between 40 and 140 counts per bin as found appropriate by trial and error.

Timing analysis was also carried out for the source GX 340+0 (Sect. 5) so that in all three sources timing analysis results could be correlated with spectral fitting results for the same selections of data along the Z-track. In the case of GX 340+0, the data used were event mode data of type E_8us_32B_14_1s which were fitted in the range 5–60 keV. The data were regrouped appropriately, again having 4–140 counts per bin.

Following presentation of results for Cygnus X-2, we present a comparison of spectral fitting and of timing analysis results for all three Cygnus X-2 like sources: Cyg X-2, GX 340+0 and GX 5-1 using our previous analyses of the *RXTE* observations of GX 340+0 made on 1997 September lasting 400 ks and the 1998 November observation of GX 5-1 spanning 95 ks (Church et al. 2006; Jackson et al. 2009). Results for the 1997 June observation of GX 340+0 are also shown.

3. Results: Cygnus X-2

The PCA lightcurve shown in Fig. 1 shows that in the first 25 ks of the observation, the source was in a period of flaring, moving on the Z-track along the flaring branch, and then onto the normal branch. The source stayed on the normal branch, until at ~100 ks it moved to the horizontal branch. It can be seen that at about 200 ks the intensity of the source had drifted upwards in comparison with the previous parts of the observation. Plotting these data on a hardness-intensity diagram revealed that the whole Z-track was moving sideways forming a "parallel track" which is often seen. For this reason, we excluded these data from our analysis to avoid superimposing data in which the source has changed. Similarly, we excluded these data from the Z-track shown in Fig. 2. A spike in the data may also be seen at ~210 ks lasting about 600 s, the nature of which is not clear, however, this event occurred in the data excluded from analysis.

Spectra were extracted at 13 positions about equally spaced along the Z-track allowing for data in some parts of the horizontal branch being sparse. Narrow ranges of hardness ratio (0.015 wide) and intensity (30 count s^{-1} wide) were defined and incorporated in good time interval (GTI) files for each selection and used to extract PCA spectra and the corresponding background files. Deadtime correction was made using a local facility PCADEAD. Systematic errors of 1% were added to each channel; it was not necessary to regroup to a minimum count in each bin to allow use of the χ^2 statistic as the count in primitive bins was already high. A response function was generated using PCARSP.

HEXTE spectra were extracted for each selection by using the same GTI files as for the PCA. The auxiliary response file (arf) of May 2000 and the response matrix file (rmf) of March 1997 were used and the rmf was rebinned to match the actual number of channels in HEXTE spectra using the FTOOLS RDDESCR and RBNRMF. The maximum energies used in the PCA and HEXTE were set at the energies at which the source flux became less than the background flux, typically 30 keV in the PCA and 40 keV in HEXTE.
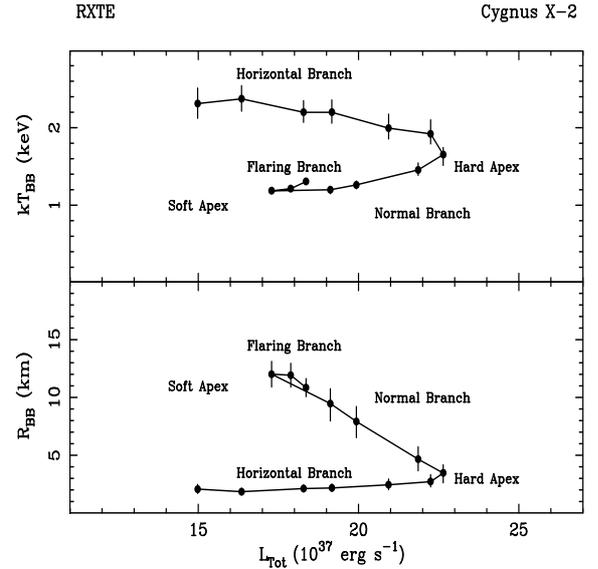
Fig. 3. *Left*: blackbody temperature (*upper panel*) and radius (*lower panel*) as a function of the total luminosity.

The extended ADC emission model was applied in the spectral fitting in the form AB ∗ (CPL + BB), where AB is absorption, CPL is a cut-off power law for Comptonization in an extended corona (Church & Bałucińska-Church 2004), and BB is the blackbody emission of the neutron star. It is well-known that the Comptonization cut-off energy in the bright Z-track sources is relatively low at a few keV compared with higher values in less luminous sources. Thus there is a limited energy range for determination of the Comptonization power law index Γ and we have taken the approach of fixing Γ at 1.7, a physically reasonable value (Shapiro et al. 1976), as adopted previously for GX 340+0 and GX 5-1 (Church et al. 2006; Jackson et al. 2009). When a best-fit was obtained, Γ was freed, but the value remained close to 1.7. In addition, a Fe line was detected at ~6.7 keV with an equivalent width of about 70 eV which showed relatively little variation along the Z-track. Good fits were obtained to all spectra, and spectral fitting results are shown in Table 1 and in Figs. 3 and 4.

In Fig. 3 we show results for the neutron star blackbody temperature kT_{BB} (upper panel) and the blackbody radius R_{BB} (lower panel) as functions of the total 1–30 keV luminosity. A clear pattern of systematic variation is evident: the temperature is lowest at ~1.3 keV at the soft apex, suggesting that the mass accretion rate $\dot{M}$ is low. At this position R_{BB} is maximum at 12 km, consistent with the whole neutron star surface being emitting. On the normal branch, the temperature rises while the blackbody radius decreases, and the temperature continues to rise on the horizontal branch.

Next in Fig. 4, we show the individual luminosities of the neutron star blackbody (L_{BB}) and the Comptonized emission (L_{ADC}) as a function of the total 1–30 keV luminosity, so that neglecting the small contribution of the line: $L_{Tot} = L_{BB} + L_{ADC}$. It can be seen that the Comptonized emission is the dominant component, ten times more luminous than the blackbody, and that as the source moves up the Z-track from the soft apex to the hard apex, this component doubles in luminosity. The X-ray intensity also, of course, increases by a similar factor and we suggest therefore that the mass accretion rate increases in this direction contrary to the widely-held view that $\dot{M}$ increases monotonically

Table 1. Spectral fitting results for Cygnus X-2: 90% confidence errors are shown.

spectrum	N_H	kT (keV)	$norm_{BB}$	R_{BB} (km)	E_{CO} (keV)	$norm_{CPL}$	χ^2/d.o.f.
Horizontal Branch							
1	1.5 ± 0.6	2.31 ± 0.20	1.96 ± 0.33	2.1 ± 0.4	7.29 ± 0.69	3.93 ± 0.41	66.7/69
2	2.0 ± 0.5	2.37 ± 0.16	1.74 ± 0.24	1.9 ± 0.3	7.00 ± 0.45	4.50 ± 0.34	77.6/68
3	2.2 ± 0.5	2.20 ± 0.14	1.67 ± 0.20	2.1 ± 0.3	6.90 ± 0.27	5.16 ± 0.33	64.3/68
4	2.3 ± 0.5	2.20 ± 0.15	1.76 ± 0.20	2.2 ± 0.3	6.70 ± 0.30	5.52 ± 0.39	82.8/68
5	2.6 ± 0.5	1.99 ± 0.16	1.51 ± 0.30	2.4 ± 0.5	6.68 ± 0.24	6.15 ± 0.45	73.4/65
Hard Apex							
6	2.7 ± 0.5	1.92 ± 0.15	1.60 ± 0.35	2.7 ± 0.5	6.43 ± 0.22	6.71 ± 0.50	52.6/55
Normal Branch							
7	2.6 ± 0.5	1.65 ± 0.12	1.43 ± 0.50	3.5 ± 0.7	5.95 ± 0.16	7.28 ± 0.60	78.4/68
8	2.4 ± 0.5	1.46 ± 0.08	1.56 ± 0.60	4.7 ± 1.0	5.68 ± 0.18	7.23 ± 0.72	56.8/58
9	1.9 ± 0.6	1.26 ± 0.05	2.54 ± 0.75	7.9 ± 1.3	5.59 ± 0.26	6.35 ± 0.85	60.3/51
10	1.6 ± 0.6	1.20 ± 0.04	2.93 ± 0.75	9.5 ± 1.3	5.45 ± 0.30	6.1 ± 0.9	74.1/70
Soft Apex							
11	0.9 ± 0.6	1.19 ± 0.03	4.55 ± 0.70	12.0 ± 1.1	5.41 ± 0.30	4.97 ± 0.85	53.6/63
Flaring Branch							
12	0.9 ± 0.9	1.22 ± 0.04	4.80 ± 1.30	11.9 ± 1.0	5.53 ± 0.60	5.05 ± 1.50	47.9/47
13	0.9 ± 0.9	1.31 ± 0.03	5.46 ± 0.6	10.9 ± 0.8	5.72 ± 0.26	4.87 ± 0.50	58.5/56

Notes. Column densities are in units of 10^{22} atom cm^{-2}; the normalization of the blackbody is in units of 10^{37} erg s^{-1} for a distance of 10 kpc, the cut-off power law normalization is in units of photon cm^{-2} s^{-1} keV^{-1} at 1 keV.
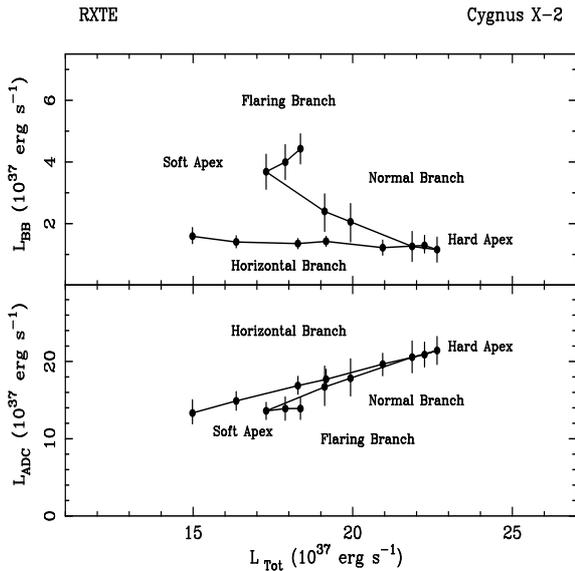

Fig. 4. Luminosities of the continuum emission components: neutron star blackbody emisssion (*upper panel*) and ADC Comptonized emission (*lower panel*).

round the Z-track in the direction HB-NB-FB (Priedhorsky et al. 1986). These variations will be discussed in more detail in the next section in terms of all 3 Cygnus X-2 like sources, given their similarity of behaviour.

4. The three sources: Cyg X-2, GX 340+0 and GX 5-1

We now present the results for Cygnus X-2 in comparison with those we previously obtained for GX 340+0 and GX 5-1 (Church et al. 2006; Jackson et al. 2009). Figure 5 (upper panel) shows the neutron star blackbody parameters. In all cases the temperature is lowest at the soft apex and rises continuously on the NB

and HB. The blackbody radius at the soft apex in all sources lies between 10 and 12 km (the dashed lines) suggesting that the whole neutron star is emitting. If this is assumed, the results provide a value of the neutron star radius based on the three measurements of 11.4 ± 0.6 km at 90% confidence. The flaring branch is characterized by some increase of temperature and a marked increase of blackbody radius.

The luminosities of the neutron star blackbody L_{BB} and of the Comptonized emission L_{ADC} are shown in the lower panel. In the variation of L_{ADC} with L_{Tot} the three sources lie on a single line on the NB, suggesting that the sources differ only in their mass accretion rate, i.e. total luminosity. We make the standard assumption of accretion physics that the total luminosity of the source L_{Tot} depends on the mass accretion rate $\dot{M}$. A single line is, of course expected, since L_{ADC} comprises a large fraction of the total luminosity. The single line does suggest that if, for example Cygnus X-2 became brighter it would appear similar to GX 340+0 in its X-ray properties. The increase of L_{ADC} in each source between the soft apex and the hard apex strongly suggests that the mass accretion rate $\dot{M}$ is increasing contrary to the standard view that $\dot{M}$ increases monotonically around the Z-track in the direction (HB-NB-FB). The observed increase of neutron star blackbody temperature on the normal branch is consistent with this as we would expect on the basis of simple accretion theory a higher temperature when more accretion flow reaches the surface of the neutron star. On the HB the luminosity of the Comptonized emission falls back towards its initial value. On the NB and HB there is an increase of blackbody temperature, but a decrease of blackbody radius. Consequently the blackbody luminosity increases less than expected for a temperature increase alone ($\sim T^4$). In flaring, there is an increase of kT_{BB}, although the flaring is weak in Cyg X-2. In all three sources, L_{ADC} remains constant or falls in flaring, indicating that $\dot{M}$ does not increase. However, the blackbody luminosity increases substantially in the strong flaring in GX 340+0 and GX 5-1 without an increase in $\dot{M}$. Thus the increase of L_{Tot} is due to the increase in L_{BB} and this must clearly be caused by an additional energy source on the neutron star, i.e. unstable nuclear burning.
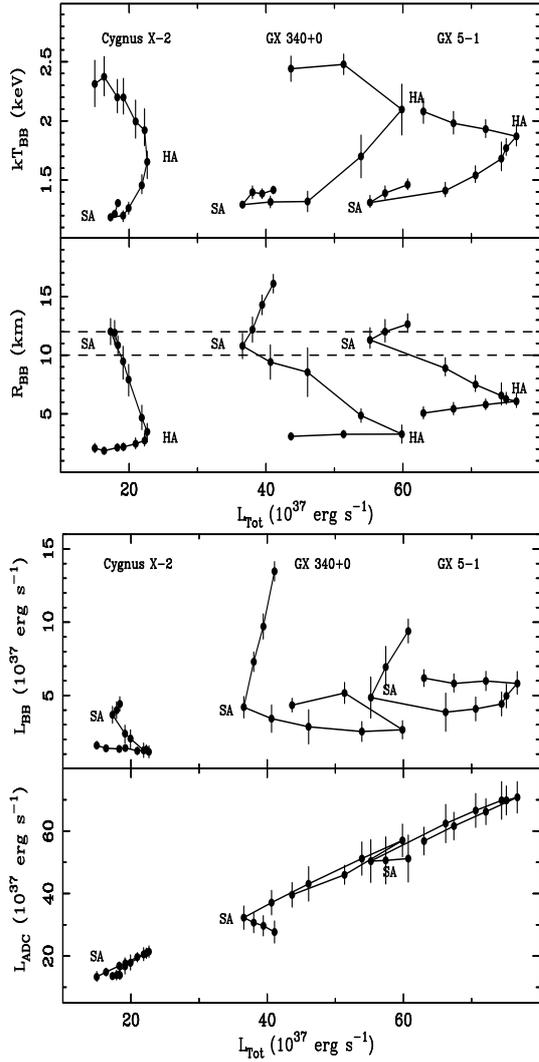
Fig. 5. *Upper panel*: blackbody temperature (*upper panel*) and radius (*lower panel*) as a function of the total luminosity; *lower panel*: the individual luminosities of the neutron star blackbody (*upper panel*) and of the Comptonized ADC emission as a function of the total luminosity (*lower panel*). The soft apex (SA) and hard apex (HA) are marked.

Fig. 6. Flux of the emitting part of the neutron star as a fraction of the Eddington flux (assumed constant) $L_{Edd}/4\pi R^2$, where $R = 10$ km.

Fig. 7. Mass accretion rate per unit neutron star emitting area $\dot{m}$.

4.1. Radiation pressure

We next view the results obtained in terms of the radiation pressure of the neutron star which we can quantify based on the spectral fitting results. In all three sources kT_{BB} increases strongly on the NB and HB, by about a factor of two. Thus radiation pressure $\sim T^4$ increases by nearly an order of magnitude. Moreover, as the source moves from the soft to the hard apex R_{BB} decreases, so that the emission of the neutron star becomes concentrated, arising from an equatorial strip, from which the emissive flux becomes high. We consider the strength of the radiation pressure in terms of the ratio of the emissive flux f to the Eddington value f_{Edd} (Sect. 1). Figure 6 shows that this ratio is initially small at the soft apex (∼0.2), i.e. sub-Eddington, but increases rapidly on the normal branch becoming equal to unity at the hard apex, then continuing to increase on the horizontal branch having super-Eddington values as high as $f/f_{Edd} = 3$ in GX 340+0. The positions on the Z-track where the sources are super-Eddington are exactly those positions where radio emission is detected indicating the presence of jets, and so we propose that high radiation pressure plays a major role in launching
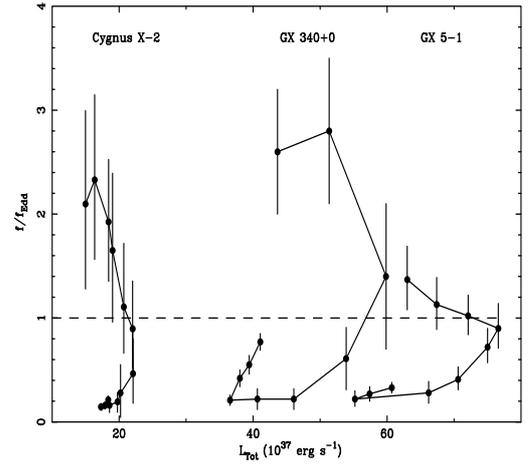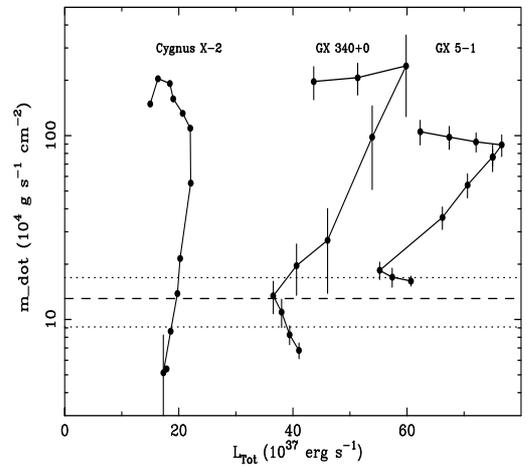
the jets, by disrupting the inner disk and diverting accretion flow into the vertical direction. In a more detailed discussion (Church et al. 2006), it is shown that the reduction in blackbody radius on the NB and HB is consistent with this disruption.

4.2. Unstable nuclear burning

In Fig. 7, we show results derived from spectral fitting for the mass accretion rate per unit area of the neutron star $\dot{m}$, using $\dot{M}$ from the 1–30 keV source luminosity and dividing this by $4\pi R_{BB}^2$. The critical value $\dot{m}_{ST}$ at which there is a transition from stable nuclear burning ($\dot{m} > \dot{m}_{ST}$) to unstable burning at smaller values of $\dot{m}$ (Bildsten 1998) is shown as a dashed line with its estimated 30% uncertainties (dotted). It may be seen that there is good agreement between the values of $\dot{m}$ at the soft apex and $\dot{m}_{ST}$ for the three sources suggesting that as a source descends from the hard apex towards the soft apex, nuclear burning becomes unstable and the result is the onset of flaring. On the flaring branch, the constancy of L_{ADC} (Fig. 5) indicates that the mass accretion rate is constant. The increase in source luminosity is due to an increase in L_{BB} at constant mass accretion rate and shows that there is an additional energy source on the neutron star not due to an increase of accretion rate, and nuclear burning is an obvious possibility. The above agreement with theory indicates that this is unstable nuclear burning. This is further discussed in
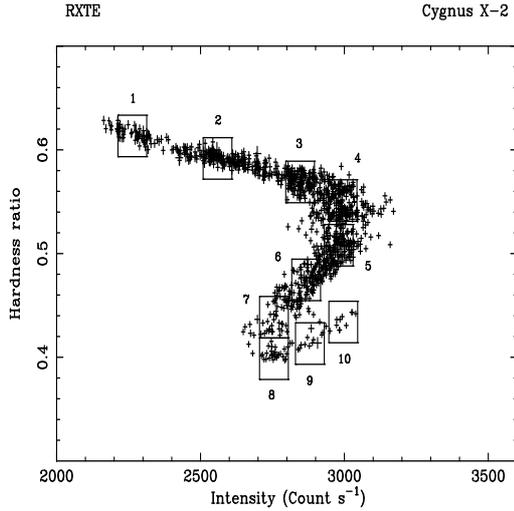
Fig. 8. Selection boxes used for fitting of the power spectra.

Fig. 9. Kilohertz QPO frequencies as a function of source luminosity for Cygnus X-2, GX 340+0 and GX 5-1.

Sect. 6. During flaring there is an increase of blackbody radius (Fig. 5) from the value at the soft apex which we take to be the neutron star radius. These increases, e.g. to 17 km in GX 340+0, indicate an expansion of the unstable nuclear burning region beyond the surface of the neutron star similar to radius expansion in the burst sources.

5. The kHz QPO

We next present results on the kHz QPO in Cygnus X-2 and GX 340+0 and compare these with our previous results for GX 5-1 (Jackson et al. 2009). The approach adopted for GX 5-1 was to use the same selections of data made around the Z-track for both spectral analysis and timing analysis, thus allowing the QPO results to be viewed in terms of the spectral and physical evolution on the Z-track. In the case of Cygnus X-2, the same general approach was used, however, because of the relative weakness of the kHz QPO, it was necessary to increase the size of the selection boxes (from those in Fig. 2) to allow detection of the QPO. Spectral fitting was again carried out for the new, larger boxes. The results of this were, however, entirely consistent with the results of Sect. 3, and were used in analysis of the QPO results. In Fig. 8 we show the new selection boxes labelled from 1 to 10. As is well-known, kHz QPO are only detected on the HB, at the hard apex and sometimes at the upper part of the NB, so the selection numbering begins at the end of the Z-track where kHz QPO are expected.

In the case of GX 340+0, timing analysis of the observation of 1997 September for which we previously presented spectral fitting results (Church et al. 2006) revealed the presence of kHz QPO on the HB. However, because of a sparsity of data in the centre of the horizontal branch, a sufficiently good dependence of kHz QPO frequency on branch position could not be obtained. Consequently the observation of 1997 June 6–10 was also analysed which was reasonably close in time to the original data. Spectral analysis as a function of Z-track position produced spectral fitting results very similar to those presented in Figs. 5–7. Better coverage of the HB was available, and we used this observation carrying out both spectral and timing analysis as a function of position on the Z-track.

In both Cyg X-2 and GX 340+0, power spectra were extracted as described in Sect. 2 and fitted in the range 150–4096 Hz, using a model consisting of two Lorentzian lines
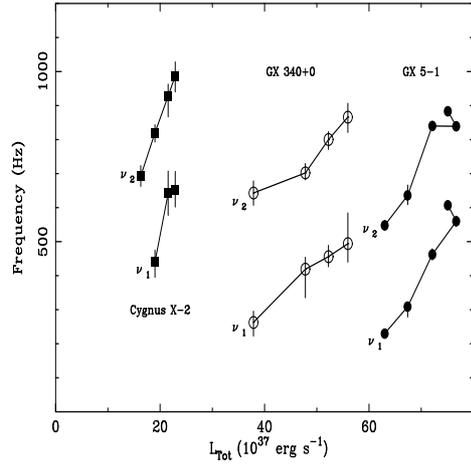
for the kHz QPO plus a power law which was able to fit the continuum adequately within this frequency range. KHz QPO could be detected on the horizontal branch only; in Cyg X-2 only the higher frequency kHz QPO could be detected in box 1 (at the end of the Z-track). Figure 9 shows the best-fit lower QPO (ν_1) and upper QPO (ν_2) frequencies as a function of the total 1–30 keV luminosity which was obtained by spectral fitting using the same model as in Sect. 4. The results for Cyg X-2 and GX 340+0 are compared with the corresponding results for GX 5-1 (Jackson et al. 2009) also shown in Fig. 9. All three sources display an increase of QPO frequency with luminosity during movement along the horizontal branch as is well-known from previous work (e.g. Jonker et al. 2000; Wijnands et al. 1998a,b). The main aim is, of course, to find the cause of the frequency change.

The frequency ν_2 is known to correspond to the orbital frequency in the accretion disk at positions a little way into the disk and we next view the results in these terms. In each case we derive the radial position r at which the Keplerian orbital frequency equals the measured QPO frequency ν, using the relation

$$2\pi\nu = \sqrt{\frac{GM}{r^3}}.$$

Thus the radius r decreases with increasing $L_{\rm Tot}$ for both upper and lower QPO. We show in Fig. 10 the radial position r not as a function of luminosity, but as a function of the ratio $f/f_{\rm Edd}$ which is a measure of the strength of the radiation pressure close to the neutron star (Sect. 4.1). The figure includes our results previously published for GX 5-1 (Jackson et al. 2009). In the case of GX 5-1, a strong increase of the QPO radius took place when the increasing blackbody temperature moving from the hard apex on the HB caused a marked increase in $f/f_{\rm Edd}$ at about $f = f_{\rm Edd}$. Super-Eddington values of the emissive flux suggest disruption of the inner disk which will increase with $f/f_{\rm Edd}$ and if the upper frequency oscillation takes place at the inner disk edge, the radius r will move outwards as observed.

In Cygnus X-2 and GX 340+0, the radial position r also increases with $f/f_{\rm Edd}$ as in GX 5-1. However, in these sources kHz QPO could only be detected on the horizontal branch so there are no QPO detections for $f/f_{\rm Edd} < 1$. In these sources, it appears that higher values of $f/f_{\rm Edd}$ are needed to produce a substantial change in QPO radius, and a possible reason for this is discussed in Sect. 6. However, the results do suggest an explanation of the kHz QPO and their variation along the HB based on our spectral fitting results. In this explanation the disk
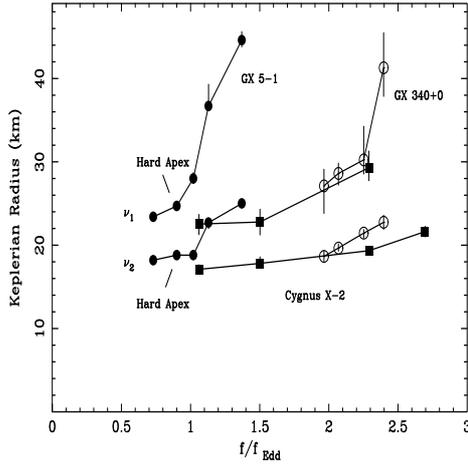
Fig. 10. Keplerian radial positions corresponding to the upper kHz QPO (ν_2) and lower kHz QPO (ν_1) as a function of the strength of the neutron star radiation pressure expressed as $f/f_{\rm Edd}$ (see text).

is disrupted on the upper normal and horizontal branches as the neutron star emissive flux becomes super-Eddington. The higher frequency QPO with frequency ν_2 (having the smaller radial position) is at all times an oscillation on the inner edge of the disk which moves outwards with increasing radiation pressure and increasing disk disruption, causing the change in the measured QPO frequency. The lower frequency QPO (ν_1) corresponding at the hard apex to $r \sim 20$ km also moves to much larger radial positions $\sim$30$-$40 km (Fig. 10). The mechanism producing this oscillation is not clear, but as its variation follows that of ν_2, it seems clear that its frequency is derived from, i.e. depends on, ν_2.

6. Discussion

We have shown that application of the extended ADC emission model for LMXB provides good fits to the spectra of all three Cygnus X-2 like Z-track sources at all positions along the Z-track. Moreover, the physical interpretation of the results is straightforward and suggests a plausible explanation of the Z-track phenomenon in this group of Z-track sources. Our explanation of the Z-track is that the soft apex is the lowest luminosity state of the source with a low value of $\dot{M}$, with emission taking place from the whole neutron star which has its lowest temperature. On the normal branch, the increase of intensity and ADC luminosity suggest an increase of $\dot{M}$ leading to heating of the neutron star and a strong increase in radiation pressure close to the neutron star as shown by the increase of $f/f_{\rm Edd}$ (Fig. 6), which continue on the HB. We suggest that this has a strong effect on the inner accretion disk causing disruption of the disk. The horizontal force may not directly remove matter from the disk, but because the unperturbed height of the inner disk in LMXB at these luminosities greater than 10^{38} erg s^{-1} is 20$-$50 km, the radiation pressure can also act in a direction close to vertical blowing away material from the upper layers of the disk. For the strongly super-Eddington fluxes that we measure close to the equatorial emitting zone of the neutron star, a fraction of the mass accretion flow may be diverted vertically upwards and be ejected from the system as massive blobs of plasma forming the jets above and below the disk. Thus we propose that high radiation pressure is a *necessary* condition for jet formation. There are large differences in luminosity between the Z-track sources with Cygnus X-2 being typically 4 times less

Table 2. The four régimes of stable or unstable nuclear burning from Bildsten (1998), showing the critical values of $\dot{m}$ that demarcate the régimes.

1 CNO unstable	2 Hot CNO stable	3 He unstable in H-rich environment	4 H, He stable
Critical values of $\dot{m}$:			
1×10^3 g cm^{-2} s^{-1} (régimes 1–2)			
5×10^3 g cm^{-2} s^{-1} (régimes 2–3)			
1.3×10^5 g cm^{-2} s^{-1} (régimes 3–4)			

luminous than Sco X-1. Although the sources are detected in radio, in Cygnus X-2 jets have not so far been imaged as in Sco X-1 (Fomalont et al. 2001), so there is the possibility that a second requirement for strong jet formation is a higher value of $\dot{M}$.

The results demonstrate that in all of the three Cygnus X-2 like Z-track sources, the flaring branch consists of a strong increase of neutron star blackbody luminosity while the Comptonized emission luminosity is constant (or decreases slightly) showing that $\dot{M}$ is constant. This indicates that the FB consists of unstable nuclear burning on the neutron star. In the theory of unstable nuclear burning (Fujimoto et al. 1981; Fushiki & Lamb 1987; Bildsten 1998; Schatz et al. 1999) the physical conditions in the atmosphere of the neutron star depend on the mass accretion rate per unit area $\dot{m}$, i.e. $\dot{M}$ divided by the emitting area. The various régimes of stable and unstable burning are shown in Table 2. The theory applies to a wide range of mass accretion rates, although it was developed to describe X-ray bursting at lower mass accretion rates, and also applies to high mass accretion rates typical of the Z-track sources, and the transition between régimes 3 and 4 takes place for luminosities of about the Eddington limit. In régime 3, burning is unstable He burning in a mixed H/He environment (Bildsten 1998) but for $\dot{m} > \dot{m}_{\rm ST}$, H and He burning of the accretion flow become stable. The agreement in all three sources of the measured $\dot{m}$ values (Fig. 7) with the critical value within its uncertainties clearly supports flaring being unstable nuclear burning. The value of $\dot{m}$ at the soft apex increases systematically with $L_{\rm Tot}$ suggesting that other, secondary effects may take place. However, the results thus provide evidence in two ways that the FB in all three Cygnus X-2 like Z-track sources consists of unstable nuclear burning. There is also an expansion of the emitting region beyond the surface of the neutron star and we propose that radius expansion may take place as it does in some X-ray bursts in lower luminosity sources.

The proposed explanation of the Z-track in the Cygnus X-2 like sources involves an increase of $\dot{M}$ between the soft apex and hard apex, and a constant $\dot{M}$ in flaring. Thus we note that this explanation departs from the often held view that the mass accretion rate increases monotonically around the Z-track in the direction HB-NB-FB.

We are also carrying out analysis of Sco X-1 like sources aimed at discovering the fundamental differences between the Cyg-like and Sco-like groups. Preliminary work on the source GX 17+2 shows that the behaviour on the normal and horizontal branches is similar to that of the Cygnus X-2 like sources. However, in flaring there is clear evidence for an increase of mass accretion rate. Thus it appears that on both the FB and NB, $\dot{M}$ increases as we move away from the soft apex, however with rather different conditions on the neutron star, i.e. different values of kT and $R_{\rm BB}$. Clearly, to fully understand the Sco X-1 like

sources extensive work will be required; however, it does appear that the difference between the two groups relates to the flaring branch, and not, for example, to inclination.

Relevant to this is the decay of the transient LMXB XTE J1701-462, which following an outburst in 2006 January, decreased by more than an order of magnitude in luminosity over about 500 days. Lin et al. (2009a) showed that the source made a transition from a Z-track source of Sco X-1 like type to Atoll behaviour, these changes being apparent from hardness-intensity diagrams. Towards the end of the decay, three X-ray bursts were observed and Lin et al. (2009b) claim that their results cast doubt on our association of the FB with unstable nuclear burning. However, the claim is not valid. Two of the bursts occurred in the time period labelled "V" by Lin et al. in which the source showed clear Atoll behaviour, having a banana branch in hardness-intensity. The other burst however occurred in period "IV" just before period V began, when flaring was weak and which in period V disappeared altogether. Although the luminosity was at that time 10% of Eddington, the authors describe the source at the period of this burst as being on the FB of a Z-track state. On the basis that it may be unlikely that bursting and unstable nuclear burning in flaring take place at the same time it was claimed that our association of the FB with unstable burning must be doubted. The argument is not correct (Lin et al. 2009a,b) as our results and model for the Z-track specifically refer to the Cygnus X-2 like sources. Thus the observation of the burst during a period when the source was described as being in a Sco X-1 like state (but normally described at such low luminosity as an upper banana state) does not cast doubt on our explanation of the Cygnus X-2 like sources in which the evidence that the FB consists of unstable burning is strong.

The kHz QPO results support the idea that high radiation pressure of the neutron star on the upper NB and HB disrupts the inner disk and that the upper QPO at frequency ν_2 is an oscillation actually at the inner edge of the disk. The inner radius is variable because of increasing disruption on the horizontal branch thus causing the well-known variation of ν_2 on that branch. The fact that the radial position associated with the QPO increases when there is also an increase of f/f_{Edd} is thus suggestive. Close to the soft apex, f/f_{Edd} is much less than unity and we do not expect the disk to be disrupted at all. Thus the inner edge of the disk will touch the neutron star, so that oscillations of the edge will probably not be possible. Thus this model for the upper frequency kHz QPO predicts that kHz QPO will not be detected on the lower normal branch, in agreement with observation.

In GX 5-1, the most luminous source, substantial change in the radial position of both upper and lower QPO takes place at $f/f_{Edd} \sim 1$, but in GX 340+0 and Cygnus X-2, larger values of f/f_{Edd} are needed which may appear surprising. However, the inner disks of the three sources have very different vertical heights and height profiles $H(r)$ and these are shown in Fig. 11 based on the standard theory of the thick disk supported vertically by its own radiation pressure (Frank et al. 2002). For each source, $H(r)$ is plotted to correspond to the luminosity at the hard apex of the Z-track where we expect there to be disruption of the inner disk. At radial positions $r < 50$ km, appropriate to the kHz QPO, $H(r)$ is rising and eventually reaches the equilibrium height of the radiatively supported disk. Also marked on the figure are radial positions corresponding to a fixed value of $f/f_{Edd} = 1.3$. Figure 10 shows that for this value, the upper kHz QPO has an equivalent orbital radius of 24 km GX 5-1 and 17 km in Cyg X-2 (there is no value of f/f_{Edd} that includes all three sources). Thus the two points plotted in Fig. 10 indicate
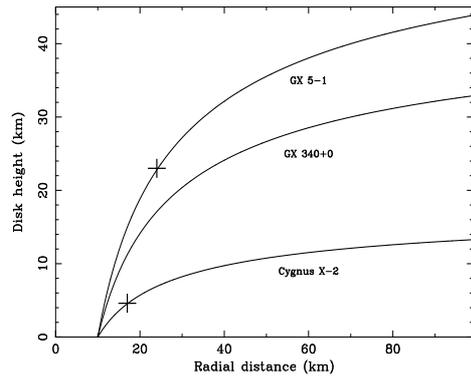

Fig. 11. Inner disk height profiles $H(r)$ for the three sources with points indicating the position of the inner disk edge in GX 5-1 and Cygnus X-2 for $f/f_{Edd} = 1.3$ (see text).

the radial positions where the QPOs occur, which we assume are the inner edges of the disk and so indicate the radial and vertical extent of disk disruption. This shows that in the brighter source GX 5-1 the disruption for a given level of radiation pressure is greater. A theoretical treatment of disruption is complex and beyond the scope of this work; however, it does not appear unreasonable that in a source with greater disk height (GX 5-1), the disruption is greater.

References

Abramowicz, M. A., & Kluźniak, W. 2001, A&A, 374, L19
Agrawal, V. K., & Sreekumar, P. 2003, MNRAS, 346, 933
Bildsten, L. 1998, in Proc NATO ASIC 515, The Many Faces of Neutron Stars, ed. R. Buccheri, J. van Paradijs, & M. A. Alpar (Dordrecht-Kluwer), 419
Church, M. J., & Bałucińska-Church, M. 1995, A&A, 300, 441
Church, M. J., & Bałucińska-Church, M. 2004, MNRAS, 348, 955
Church, M. J., Halai, G. S., & Bałucińska-Church, M. 2006, A&A, 460, 233
di Salvo, T., Farinelli, R., Burderi, L., et al. 2002, A&A, 386, 535
Done, C., Życki, P., & Smith, D. A. 2002, MNRAS, 331, 453
Fomalont, E. B., Geldzahler, B. J., & Bradshaw, C. F. 2001, ApJ, 558, 283
Frank, J., King, A. R., & Raine, D. J. 2002, Accretion power in astrophysics, third edition (Cambridge University Press)
Fujimoto, M. Y., Hanawa, T., & Miyaji, S. 1981, ApJ, 247, 267
Fushiki, I., & Lamb, D. Q. 1987, ApJ, 323, L55
Hasinger, G., & van der Klis, M. 1989, A&A, 225, 79
Hasinger, G., van der Klis, M., Ebisawa, K., Dotani, T., & Mitsuda, K. 1990, A&A, 235, 131
Jackson, N. K., Church, M. J., & Bałucińska-Church, M. 2009, A&A, 494, 1059
Jonker, P. G., van der Klis, M., & Wijnands, R. 2000, ApJ, 537, 374
Kuulkers, E., & van der Klis, M. 1995, A&A, 303, 801
Lin, D., Remillard, R. A., & Homan, J. 2009a, ApJ, 696, 1257
Lin, D., Altamirano, D., Homan, J., et al. 2009b, ApJ, 699, 60
Miller, M. C., Lamb, F. K., & Psaltis, D. 1998, ApJ, 598, 791
Mitsuda, K., Inoue, H., Nakamura, N., & Tanaka, Y. 1989, PASJ, 41, 97
Psaltis, D., Lamb, F. K., & Miller, G. S. 1995, ApJ, 454, L137
Priedhorsky, W., Hasinger, G., Lewin, W. H. G., et al. 1986, ApJ, 306, L91
Schatz, H., Bildsten, L., Cumming, A., & Wiescher, M. 1999, ApJ, 524, 1014
Schulz, N. S., Huenemoerder, D. P., Ji, L., et al. 2009, ApJ, 692, L80
Smale, A. P., & Kuulkers, E. 2000, ApJ, 529, 702
Smale, A. P., Homan, J., & Kuulkers, E. 2003, ApJ, 590, 1035
Stella, L., & Vietri, M. 1998, ApJ, 492, L59
Walter, F. M., Mason, K. O., Clarke, J. T., et al. 1982, ApJ, 253, L67
White, N. E., & Swank, J. H. 1982, ApJ, 253, L61
Wijnands, R., Homan, J., van der Klis, M., et al. 1998a, ApJ, 493, L87
Wijnands, R., Méndez, M., van der Klis, M., et al. 1998b, ApJ, 504, L35
van der Klis, M., Stella, L., White, N. E., Jansen, F., & Parmar, A. N. 1987, ApJ, 316, 411
Xiang, J., Lee, J. C., Nowak. M. A., Wilms, J., & Schulz, N. S. 2009, ApJ, 701, 984